Negative nonlocal vicinity resistance of viscous flow in a two-dimensional electron system

Wei-Jie Ji [1,2] Shu-Yu Zheng,[3] Li Lu,[3] Kai Chang,[1,2,4] and Chi Zhang [1,2,4,*]

[1]*State Key Laboratory of Superlattices and Microstructures (SKLSM), Institute of Semiconductors,
Chinese Academy of Science, P.O. Box 912, Beijing 100083, China*
[2]*College of Material Science and Opto-Electronic Technology, University of Chinese Academy of Sciences, Beijing 100190, China*
[3]*Beijing National Laboratory for Condensed Matter Physics, Institute of Physics, Chinese Academy of Sciences, Beijing 100190, China*
[4]*CAS Center for Excellence in Topological Quantum Computation, University of Chinese Academy of Sciences, Beijing 100190, China*

We perform a quantum transport study of Hall viscous liquid in multiterminal narrow Hallbar devices of a high-mobility two-dimensional electron system (2DES) in GaAs/AlGaAs heterostructure. In the nonlocal transport measurements of vicinity geometry under magnetic fields (B), we observe that the absolute negative magnetoresistance (R_{xx}) value ($R_{min} < 0$) and the corresponding magnetic field (B_{min}) are both inversely proportional to the adjacent Hallbar arm distance (L). The occurrence of negative resistance is dependent on the characteristic lengths of the devices and the electron flow direction under B-fields. The minimal resistance R_{min} occurs when the cyclotron radius R_C approximates L. Multiples of high-order (nth-order) $R_{min,n}$'s persist from low to high magnetic fields in a large sample size of $L = 5$ μm. Our experimental study reveals the transport behaviors in the vicinity regime, where the negative resistances depict viscous electronic flows in the high-mobility 2DES. In addition, the negative and high-order minimal resistances expand to a magnetic field of several kGs.

I. INTRODUCTION

A two-dimensional electron system (2DES) in GaAs/AlGaAs heterostructures provides an ideal platform for the study of novel quantum states with diverse electron-electron interactions, for instance integer quantum Hall effects (IQHEs) [1] and fractional quantum Hall effects (FQHEs) [2]. In a high-mobility 2DES (or metals), the mean free path of electron-electron collision is much shorter than that of electron-phonon and electron-impurity scattering ($l_{ee} \ll l_{mfp}$). In the Ohmic regime (diffusion), the sample size (l) is larger than the mean free path of electron-phonon collisions, i.e., $l > l_{mfp}$, and the devices obey Ohm's law. The quantum analog of the classical hydrodynamics theory described by the Navier-Stokes equation can effectively portray the microstructure confinements of the electron flows with $l_{ee} < l < l_{mfp}$ (in the hydrodynamic regime) [3–6]. In a sufficiently narrow confinement (from the hydrodynamic to the ballistic transport regime, or in an even narrower regime), viscous flow provides a major contribution to the conductance that exceeds Landauer's ballistic limit (superballistic conductance) at low temperatures ($T > 0$) [7]. Moreover, the long-wavelength and low-energy behaviors of electron systems in the quantum hydrodynamic regime conform to the Fermi liquid theory under the condition of $l_{ee} > l$ (or λ, the wavelength), where $l_{ee} \sim v_F \frac{E_F}{(k_B T)^2}$ [8], e.g., the electrons on [3]He [9]. Due to the very small amount of impurities in the very high-mobility 2DES

(i.e., the high-mobility electron channel in GaAs/AlGaAs heterostructures), the length of electron-electron collision, l_{ee} (i.e., the phase-coherent length of electrons), is much smaller than the mean free path of electron-phonon scattering, $l < l_{ee} \ll l_{mfp}$, which corresponds to the superballistic transport regime. The strongly correlated electron system in transport with various types of collisions is an analog of viscous fluids [10–17], which has been revealed in ambient theoretical and experimental studies in two-dimensional systems [18–26]. Moreover, the hydrodynamics in electronic viscous flows extends to other systems in condensed matter, such as the topological phases [27,28].

The electron liquid is described as an analog of Poiseuille flows in solid [11], which is detected in the temperature (T)-dependent nonlinear transport in a 2DES with a confinement [10]. Viscous Poiseuille flows in the spatial distribution in graphene and nanoscale structure devices are detected by means of scanning microscopy based on carbon nanotube single-electron transistor (SET) and high-resolution nitrogen-vacancy (NV) center techniques [29,30]. Experimental studies reveal the hydrodynamics of the highly viscous fluid in graphene in electronic and thermoelectric transport [23,31], in a 2DES in the ballistic regime [32,33], and in other quantum materials [34]. In addition, theoretical studies propose various techniques to probe the viscosity of electron fluids, such as nonlocal transport, scanning probes, etc. [35]. The viscosity in electron liquids produces the vorticity of shear flows, leading to the backflow of the current and the generation of negative nonlocal resistance [18]. At present, a nonlocal transport study of a high-mobility 2DES in GaAs submicron-scale structures in the quantum hydrodynamic regime remains lacking [35].
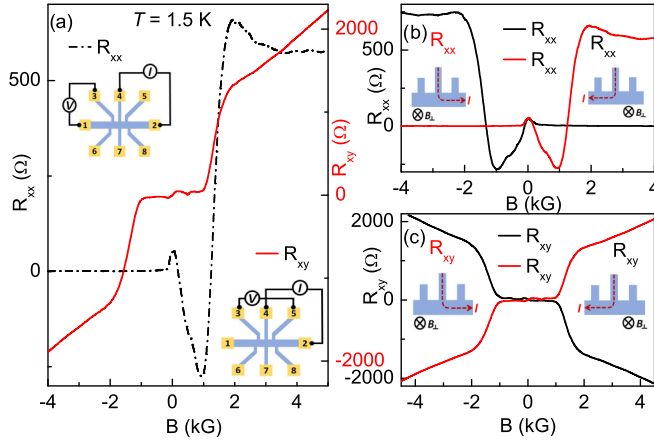
*zhangchi@semi.ac.cn

FIG. 1. (a) Longitudinal resistance (black dash-dotted curve) and Hall resistance (red solid curve) of S1 measured at 1.5 K. The insets show the configurations of R_{xx} and R_{xy} measurements, respectively. (b) Clockwise (black) and counterclockwise (red) R_{xx} curves show mirror image features of each other with respect to the $B = 0$ axis. (c) Clockwise (black) and counterclockwise (red) R_{xx} curves show mirror image features of each other with respect to the $B = 0$ axis.

The transport measurements of a 2DES have reported robust resistance maxima at very low B-fields that stem from 2D electron liquids [10]. According to the recent research of magnetoresistances at very low B-fields, the sharp decrease of longitudinal resistance can be accounted for by the viscous flow in a 2DES [36–38]. A subsequent theoretical report proposes that negative resistance occurs when the cyclotron radius $R_C < L$, even when $l_{ee} > L$ or w (sample sizes), where the magnetoresistances are expressed as a function of cyclotron frequency $\omega_C \equiv eB/m^*$ [19]. It is put forward that the nonlocal resistance of various geometries can effectively prove the viscosity electron flows [35], and can demonstrate the criterion of the whirlpool occurrence [39]. Our experimental study reveals negative resistance (NR) in I-V measurements of vicinity geometry at a perpendicular B which corresponds to the cyclotron resonance (CR). Moreover, the higher-order minimal longitudinal resistances persist at high $B \sim 2-4$ kG.

II. METHOD

Our high-quality 2DEG wafer with a GaAs/AlGaAs heterojunction is grown by molecular-beam epitaxy (MBE). The high-mobility ($\mu \sim 3 \times 10^6$ cm^2/V s) electron channel in a one-side modulation-doped heterojunction is about 200 nm beneath the sample surface, and the density is $n_e = 1.8 \times 10^{11}$ cm^{-2} after LED illumination at low temperature. Our multiterminal Hallbar devices, which are fabricated with electron-beam lithography (EBL) and plasma etching, are shown in the schematic diagram in the insets of Fig. 1(a). The Hallbar widths (w) are $\sim 3-8$ μm, the probe arm widths (d) are about $0.3-0.6$ μm, and the spaces between the two nearby probes (L) are about $\sim 0.8-5.0$ μm, as shown in Table I. To achieve an optimal guide of the unidirectional electron flows under B-fields, we fabricate the devices with relatively small d's. The multiterminal Hallbars of different dimensions are denoted as S1, S2, S3, and S4, respectively. The dimensions

TABLE I. Dimensional parameters of the multiprobe Hallbar structures or devices.

	w (μm)	d (μm)	L (μm)
S1	3	0.3	0.8
S2	8	0.6	1.2
S3	8	0.5	1.5
S4	8	0.5	5.0

are $w = 3$ μm, $d = 0.3$ μm, $L = 0.8$ μm in S1; $w = 8$ μm, $d = 0.6$ μm, $L = 1.2$ μm in S2; $w = 8$ μm, $d = 0.5$ μm, $L = 1.5$ μm in S3; and $w = 8$ μm, $d = 0.5$ μm, $L = 5$ μm in S4. The parameters (i.e., w, d, and L) of the device structures are illustrated in the left inset of Fig. 3(a).

All magnetotransport measurements are performed by means of the standard low-frequency (at $f = 17$ Hz) lock-in techniques with an external current (I) of $\sim 0.1-1$ μA applied to the sample, in a cryogen-free cryostat at a base T of 1.5 K. The magnetic field consists of a perpendicular B and a parallel magnetic field, both of which are provided by superconducting coils of magnets.

We include different I-V configurations in our nonlocal transport measurements to reveal the viscosity in the electron fluidity, as illustrated in Figs. 1(a), 1(b) and 1(c), respectively. The two insets of Fig. 1(a) depict a configuration (C1) for the nonlocal measurements of longitudinal resistance (R_{xx}, or nonlocal resistance of vicinity geometry R_V) and transverse resistance (R_{xy}), respectively. The eight Ohmic contacts of the multiterminal Hallbar are labeled by numerals (from 1 to 8). The external current is applied from contact 4 to 2, whose orientation is counterclockwise. Another configuration (C2) for the I-V measurements via an external current in a clockwise direction (from contact 4 to 1) and a voltage drop between two contacts in vicinity is shown in the right insets of Figs. 1(b) and 1(c).

III. EXPERIMENTAL RESULTS

The longitudinal resistance (R_{xx}) and the Hall resistance R_{xy} at $T \sim 1.5$ K are illustrated in Fig. 1(a). There is a small spike (above zero) in R_{xx} (black dashed-dotted curve) at around zero magnetic field (B), and the R_{xx} features at $B < -0.2$ kG stay very close to zero. At $B > 0.2$ kG, the longitudinal resistance shows negative values, and the minimum $R_{xx} < -300$ Ω occurs at $B \sim 0.9-1.0$ kG. The associated R_{xy} (red solid curve) of the nonlocal transport also remains very low (about -20 Ω) in the regime of $-0.9 < B < -0.2$ kG, which deviates from the regular Hall resistivity in transport and is attributed to the quenching of quantum Hall resistivity in the mesoscopic structures [40].

The curves of R_{xx} in the two configurations [in Fig. 1(b)] are the mirror images of each other with respect to the $B = 0$ axis. The left (right) inset shows the configuration with the counterclockwise (clockwise) current direction with respect to B. Likewise, the R_{xy} features of the two configurations of measurements are the mirror images of each other in Fig. 1(c).

The R_{xx} and R_{xy} data in Figs. 1(b) and 1(c) clearly illustrate the relation between the current flow and the B orientations. R_{xx} in the nonlocal transport is defined as R_{NL} [35]. The
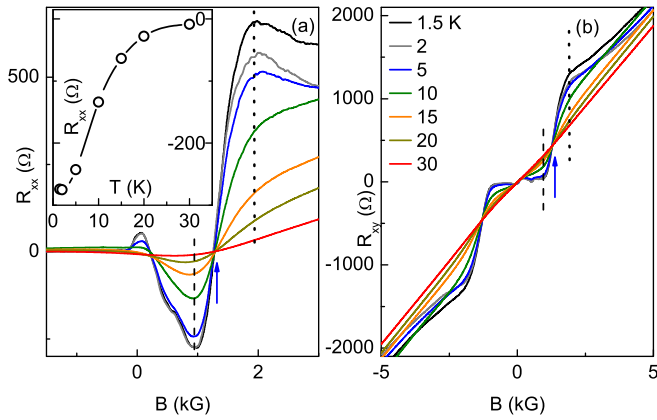
FIG. 2. (a) Temperature-dependent R_{xx} of S1 at $T \sim 1.5-30$ K. The inset shows R_{xx} (at $B \sim 0.96$ kG) vs T. (b) T-dependent R_{xy} in the regime of $T \sim 1.5-30$ K.

FIG. 3. (a) The Hallbar (S1, S2, and S3) size-dependent I-V (R_{xx}) under low B-fields at 1.5 K. The left inset shows the dimensions (w, L, and d) of the multiprobe Hallbar devices (S1, S2, and S3), which are consistent with the parameters in Table I. The inset on the right exhibits the relations of the minimal R_{xx} (R_{min}, left axis) vs $1/L$ and corresponding B-field (B_{min}, right axis) vs $1/L$. Both R_{min} and B_{min} are proportional to $1/L$. (b) The zoomed-in features of the negative nonlocal resistance of S1 at 1.5 K. Black, blue, and red dashed lines highlight the minimal features that are centered near $B = 0.96$, 0.48, and 0.24 kG, respectively.

negative resistance (NR) [red curve in Fig. 1(b)] occurs at the positive B with the counterclockwise (CCW or C1) current (left inset), and the resistance declines to about zero at $B < -0.2$ kG. Inversely, the negative resistance [black curve in Fig. 1(b)] occurs at the negative B with the clockwise (CW or C2) current (right inset), and the resistance is close to zero at $B > 0.2$ kG. So the "diode"-like features of the nonlocal voltage probing with respect to B-fields indicate the electron flows' orientation under magnetic fields: $\Delta V < 0$ obtained by the V-probe denotes the counterflow due to the current whirlpool [23], but the current flows cannot pass through the V-probe at the opposite B-direction (or at the other side of the current injection channel).

Temperature-dependent magnetoresistances in the I-V measurements are exhibited in Figs. 2(a) and 2(b). In panel (a), the minimal values of R_{xx} (R_{min}) increase with T, and the amplitudes of the spike at $B = 0$ and the shoulder at $B \sim 2$ kG are weakened with increasing T. The relation of R_{min} versus T is displayed in the inset of panel (a). The minimal (NR) R_{xx} value grows with T, $R_{xx} < -250$ Ω at $T < 2$ K, and approaches zero at around 30 K.

The minimal resistance $R_{min,xx}$ [in Fig. 2(a)] and the corresponding shoulder features in R_{xy} are observed at $B \sim 0.96$ kG, denoted by the dashed lines. The curve at base T is more complex than that at higher T, and the shoulder occurs at about $B \sim 0.48$ kG, which will be analyzed in the descriptions of Fig. 3(b). The maximal longitudinal resistance R_{max} [in Fig. 2(a)] occurs at about $B_{max} \sim 2B_{min}$, in correspondence to the shoulder features of R_{xy} at low T [in Fig. 2(b)]. Moreover, the crossing point (fixing point) at various temperatures appears at 1.28 kG, which is about $B_{crossing} = (4/3)B_{min}$ [highlighted by the blue arrows in both Figs. 2(a) and 2(b)]. The relations between B_{min}, $B_{crossing}$, and B_{max} are valid in all the submicron-scale devices (i.e., S1, S2, and S3). The uniform electron density in the hydrodynamic transport in S1 ($\bar{n} \sim 1.6 \times 10^{11}$ cm^{-2}) is estimated from the slope of R_{xy}, which is only a little smaller than n in the wafer. So the crossing point is determined by the homogeneous electron density and cyclotron resonance (CR).

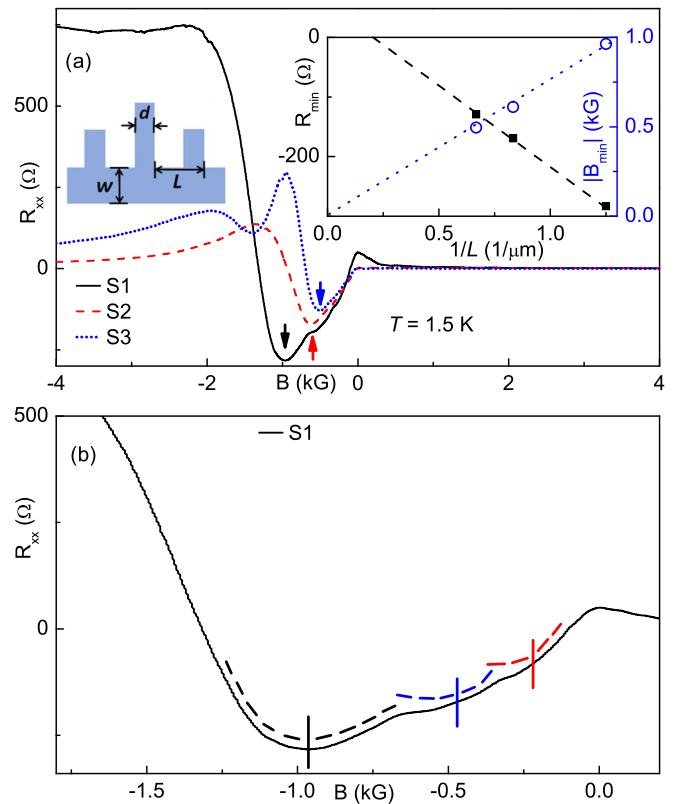We note that the T-dependence of R_{xx} (in C1) shows evident asymmetry with regard to the $B = 0$ axis, and NR is

very robust at the $B > 0$ side [in Fig. 2(a)], which indicates the vicinity effect from the electron flows between the applied current and the voltage probing. The T-dependent R_{xy} curves do not display evident asymmetry in either the regime of $B > 0$ or $B < 0$. Because the current flow crosses over with the voltage loop, the features of electron fluidity are not very robust in Hall resistance. Furthermore, we notice that the curves at $T \leqslant 5$ K are more complicated than those at higher T: the shoulder occurs at $B \sim 0.48$ kG, which corresponds to $1/2$ of the B_{min} value. The features are illustrated in Figs. 1(a) and 1(b) in both C1 and C2.

To explicate the relation between the dimensions of the devices and the negative magnetoresistance, we illustrate the size-dependent transport results of the devices in Fig. 3(a). The sample dimensions are displayed in the left inset with w, L, and d listed in Table I. The R_{xx} curves at the low B-field of S1, S2, and S3 are denoted by the black solid, red dashed, and blue dotted lines, respectively, and the arrows (of different colors) highlight minimal R_{xx} (R_{min}) at different B ($|B_{min}|$) of S1, S2, and S3. The relations of R_{min} (left axis) versus $1/L$ and B_{min} (right axis) versus $1/L$ are shown in the

right inset: B_{min} is proportional to $1/L$, and the corresponding R_{min} is linear to $1/L$. The slope of the blue curve $B_{min}L$ is about 0.67 kG μm, which is relative to the cyclotron radius $R_C = l_B^2 k_F$, where $l_B = \frac{25.7}{\sqrt{B\,[T]}}$ nm is the magnetic length, and $R_C = \frac{0.05 \times 1.35}{B\,[T]} = \frac{0.7}{B\,[kG]}$ μm. Therefore, NR occurs when the Hallbar arm distance is equal to R_C. We could further deduce the intersection point at $1/L = 0.2$ μm^{-1} of the dashed line and $R_{xx} = 0$, indicating the maximal size ($L \leqslant 5$ μm) of the occurrence of the negative resistance. The negative resistances are not relative to the Hallbar widths w or the arm (probe) widths d.

In addition, there are two sets of minima (and maxima) in the nonlocal magnetoresistances of S3, whose sizes are larger than those of S1 and S2. Not only a minimum (maximum) occurs at $B \sim 0.45$ kG ($B \sim 0.9$ kG) in correspondence to $R_C = L$ ($2R_C \sim L$), but also a minimum (maximum) is located at about $B \sim 1.3$ kG ($B \sim 1.8$ kG) corresponding to $3R_C \sim L$ ($4R_C \sim L$). The minimum at $L \sim 3R_C = 2(n + 1/2)R_C$ can be understood as the first-order term (with $n = 1$) of NR at $R_C = L$.

At base T, the zoomed-in NR of S1, which has the smallest size, is relatively complex, as shown in Fig. 3(b). The minima in the NR trace occur at $B \sim 0.96$, 0.48, and 0.24 kG, denoted by the black, blue, and red color bars, respectively. The minima are correspondent to the prime (first-order), second-harmonic ($R_C = 2L$), and fourth-harmonic ($R_C = 4L$) frequency of the negative resistance (at $R_C = L$). So the curve at $T < 5$ K can be considered as the superposition of the frequency multiplications. The high-order features are much weaker than the prime, as they originate from the once ($R_C = 2L$) and twice ($R_C = 4L$) rebounding between the arms with a distance L. Similar features in zoomed-in NR [in Fig. 2(a)] are robust at $T \leqslant 5$ K, but disappear at $T > 10$ K, for l_{ee} decays so dramatically with temperature that the hydrodynamic conditions cannot be satisfied.

In the larger sized sample structure S4 (with $d = 0.5$ μm and $L = 5$ μm) in the transitional regime of ballistic and hydrodynamic transports, the negative longitudinal resistance R_{xx} becomes invisible, as is shown in Fig. 4, which is consistent with the deduction from the size-dependent study, illustrated in Fig. 3(a). Distinct from the nearly vanished R_{xy} features in I-V measurements (at small B) in the small sized devices [Fig. 1(b)], the Hall resistivity curve of S4 shows indications of plateau features at $-1 < B < 1$ kG, which are highlighted by the blue dots in the top inset of Fig. 4.

Furthermore, many B-periodic oscillations (marked by the bars) occur in both R_{xx} (black color bars) and R_{xy} (red color bars) at 1.5 K (in Fig. 4). Thus the features of longitudinal resistance and Hall resistivity of the nonlocal I-V study can be understood as the superposition of the quantum hydrodynamic features and the B-periodic oscillations. The B-periods of minima in R_{xx} are about $\Delta B \sim 0.28$ kG, which endure from zero to high B fields. The Hall resistivity features are antisymmetric to the $B = 0$ axis: the maxima of R_{xy} at $B > 0$ are antisymmetric to the minima of R_{xy} at $B < 0$, as denoted by the red bars.

At $B > 0$, the minima of R_{xx} correspond to the maxima of R_{xy}, whose periods are about $\Delta B \sim 0.28$ kG. According to our analysis of the results of submicron-scale structures

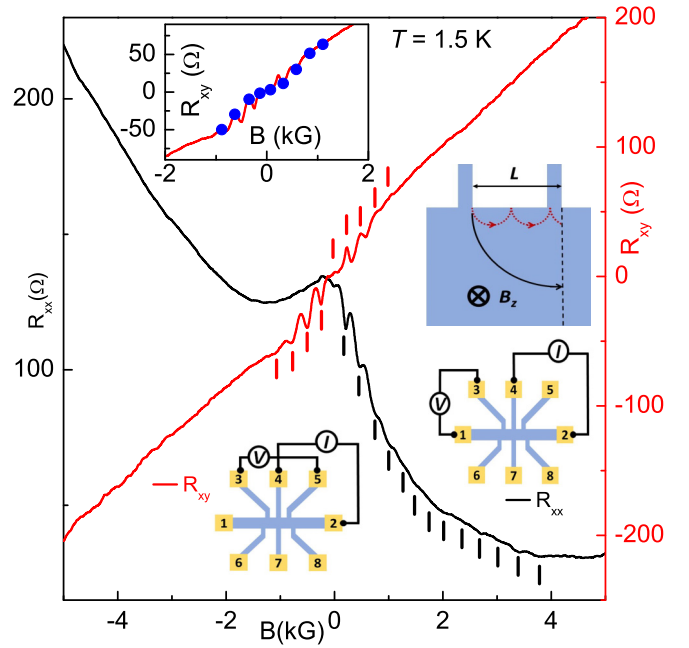FIG. 4. Longitudinal resistance and Hall resistivity in the I-V measurements of structure S4 at 1.5 K. Top inset: zoomed-in R_{xy} features at $-2 < B < 2$ kG (red curve), and the blue dots highlight the indication features of viscous electron fluids at $-1 < B < 1$ kG. The configurations of R_{xx} and R_{xy} in nonlocal I-V measurements are displayed in the inset at the bottom-right corner and the bottom inset, respectively. In addition, the trajectory of the electron flows under magnetic fields with the relation of $2(n + \frac{1}{2})R_C = L$ is shown in the upper right inset, where the zeroth order ($n = 0$) is displayed by the black solid curve and the integer nth order is exhibited by the red dashed curve.

(S1, S2, S3), the relation $R_C = \frac{0.7}{B\,[kG]}$ μm also holds in the larger structure of S4, because $R_C = \frac{0.7}{0.28} = 2.5$ μm, which is about one-half of the size of the arm distance $L = 5$ μm. In S1, S2, and S3, the first-order $B_{max,1}$ is twice that of $B_{max,0}$, and the second order of B_{min} ($B_{min,2}$) is triple that of $B_{min,0}$. So the B-period between the adjacent $B_{max,n}$ and $B_{max,n+1}$ (or adjacent $B_{min,n}$ and $B_{min,n+1}$) equals B_{max}, which corresponds to the relation of $L = 2R_C$. The first black bar from the left corresponds to $B_{min,0} \sim 0.14$ kG, and the higher order $B_{min,n}$ stays robust until $n = 14$.

In general, the high-order minimal features of R_{xx} in the large sized device (S4) are congruent with the negative resistances (R_{xx}) of submicron structures (S1, S2, and S3). The NR features are very robust at about $R_C = L$, and the maximal resistance at $2R_C = L$ corresponds to the resonance from the collisions (in structures S1, S2, and S3). Moreover, the nonlocal NRs also occur at $2(n + \frac{1}{2})R_C = L$ (n is an integer number), whose trajectory curves are illustrated in the right inset of Fig. 4.

The nonlocal magnetoresistances of S4 show explicit B-periodic oscillations (in Fig. 4), which is in stark contrast with the $1/B$-periodic oscillations of geometric oscillations [41]. The minima of nonlocal R_{xx} involve a different mechanism from the maxima, which is even more evident in S4. The minima of R_{xx} occur under the condition of $2(n + \frac{1}{2})R_C = L$,

but the maxima do not bear the relation of $2nR_C = L$ in S4, nor do they form the exact relation of $2R_C = L$ in S1, S2, or S3. The profile of the nonlocal R_{xx} at $B > 0$ is understood as the superposition of a smooth envelope and many high-order NRs (or minima), which originate from the shear viscosity in hydrodynamic flow.

IV. DISCUSSION

In our analysis of the Hall viscosity of electron liquid, it is important to compare the various characteristic lengths. Based on the Landau theory, l_{ee} is in the order of $\sim v_F \frac{E_F}{(k_B T)^2}$. The mean free path for electron-electron collision in the hydrodynamic regime of graphene is expressed as $l_{ee}^{-1} = \frac{\pi k_F}{N}(\frac{k_B T}{E_F})^2 \ln(\frac{2E_F}{k_B T})$, which can be estimated as $l_{ee} \sim 1.0~\mu m$ with the parameters in our 2DES samples [42]. But the calculation does not take into account the scattering rate between the electrons and the disorder, $\frac{1}{\tau_{2,0}}$, which is independent of temperature. As a result, the quantum lifetime of an interacting 2DES with electron-electron collisions is deduced as $\frac{\hbar}{\tau_{2,ee}} = A_{ee}^0 \frac{T^2[\ln(2E_F/T)]}{E_F} + \frac{\hbar}{\tau_{2,0}}$ [43]. The value of the first term on the right-hand side of the equation is about 0.26×10^{11} s^{-1}, and $\tau_{2,ee}^{-1} \sim 1.26 \times 10^{11}$ s^{-1} by estimating $\tau_{2,0}^{-1} \sim 1 \times 10^{11}$ s^{-1} [33]. The mean free path of electron-electron collision is about $l_{ee} \sim 1.5~\mu m$, which is in a reasonable range of 2DES with a regular density [33].

The negative nonlocal voltage (or resistance) comes from the shear viscosity that results in the vorticity and the backflow near the side of the external current path [18]. The kinematic viscosity of the 2DES is about $\nu = v_F l_{ee}/4 \approx 0.07$ m^2/s, which is relatively close to that of Dirac fermion fluid in graphene [23,42], but smaller than that of a high-density 2DES [32]. Because of the high mobility of the 2DES channel, the vorticity diffusion length $D_\nu = \sqrt{\nu\tau} \approx 4.2~\mu m$, which is much larger than that in graphene samples [24]. The nonlocal hydrodynamic transport is dependent on the geometry of the measurement configurations: the NR in the half-plane sample results from the viscosity in the absence of current whirlpools, but the negative nonlocal resistance of vicinity geometry indicates backflows near the current injections, and the whirlpool occurrence is determined by D_ν. In our sample structures, the large D_ν meets the criterion of the whirlpool occurrence in electron hydrodynamics in the sample of vicinity geometry: $D_\nu > w/\sqrt{2\pi}$ and the shear viscosity of $\nu > w^2/(2\pi^2\tau) \sim 0.015$ m^2/s [39]. As shown by the analysis in theory and calculation on vicinity geometry, at a sufficiently small L, the existence of NR with whirlpools (or backflows) is independent of D_ν [39].

Recent experimental reports mainly focus on the viscous flow in graphene. But the different phenomena between the 2DES and graphene suggest distinct mechanisms involved. First of all, the temperature regime of the highly viscous electron fluid in graphene is much larger than the electron flows in the 2DES in GaAs/AlGaAs heterostructures. While high viscosity persists from 1 K to above 200 K in single-layer graphene (SLG) or double-layer graphene (DLG) [23], the viscous electron flows of the high-mobility 2DES in GaAs could persist in electronic transport from 1 K to about 30 K.

Because the scattering of electrons is mainly caused by the defects of SLG or DLG, the mobility varies a little from low to high T. In contrast, the electron-phonon interactions in a 2DEG in GaAs/AlGaAs heterostructures smear out below 4 K, so the mobility increases dramatically at very low T.

An ensuing question concerns the T-dependent nonlocal resistances of a high-mobility 2DES. A theoretical proposal claims the resistivity is inversely proportional to the square of temperature ($R \sim 1/T^2$) in electron liquid [12]. However, in the absence of B, our T-dependent nonlocal transport results deviate from the relation $R \sim 1/T^2$ [12], hence they diverge from the observation of graphene [24], because the Gurzhi effect not only largely relies on the geometry and configurations of the transport measurements [44], but it also pertains to boundary conditions [35].

In the T-dependent superballistic transport (in the absence of B) in the viscous point contact (VPC) of graphene, the extracted viscous conductance (G_ν) is proportional to the width of VPC confinements w_{VPC} [42]. It is analyzed in a theoretical model that the viscous conductance at base T is proportional to the square of the confined VPC width in graphene [7]. But the nonlocal vicinity R_{xx} (or R_V) curves exhibit that the negative R_V (and shear viscosity) occurs as a function of ω_C (or B), and the minima of R_V are proportional to $1/L$. The discrepancy between our experimental results and those in Ref. [42] originates from the differences in geometries and configurations in measurements.

In our submicron scale devices (S1, S2, and S3), the longitudinal resistance (R_{xx}) features of MR measurements (not I-V measurements) at the low magnetic fields of $B \sim 0$ are negative ($R_{xx} < 0$). But in larger sized Hallbar structures [45], the R_{xx} trace exhibits a colossal peak in the vicinity of $B \sim 0$, which is in agreement with Ref. [10]. In our structure size in between the submicron and several-micron scale (i.e., S4), a distinct peak R_{xx} above zero is observed, which is the case in the transition regime between submicron and large-scale structures. Meanwhile, the nonlocal I-V curves exhibit transitional features between the submicron and 5-micron structures.

V. CONCLUSION

In summary, we observe negative nonlocal magnetoresistance (NNMR) in the superballistic transport regime in multiterminal Hallbar devices, which reveals the Hall viscosity of electron flows. The current flows are well defined in our experiments because the unidirectional external current is applied via the narrow Hallbar arms. The occurrence of absolute negative resistance (or voltage) of vicinity geometry originates from the counterflow generated by the shear viscosity in 2DES, and the NNMR (at B-fields) is determined by the electron flow of cyclotron motions and external B-field directions. Moreover, in the devices of micron scales that correspond to the ballistic transport, we unexpectedly observe B-periodic high-order minima enduring from low to high B. Our size-dependent study provides systematic evidence for the Hall viscous flow. The nonlocal magnetotransport in the superballistic regime may stimulate theoretical discussion of the quantum hydrodynamic fluids with finite viscosity.

[1] K. v. Klitzing, G. Dorda, M. Pepper, P. Ai, and R. Letters, Phys. Rev. Lett. **45**, 494 (1980).

[2] D. C. Tsui, H. L. Stormer, and A. C. Gossard, Phys. Rev. Lett. **48**, 1559 (1982).

[3] L. D. Landau and E. M. Lifshitz, *Course of Theoretical Physics: Fluid Mechanics* (Pergamon Press, New York, 1987).

[4] G. K. Batchelor, *An Introduction to Fluid Dynamics* (Cambridge University Press, Cambridge, UK, 1967).

[5] K. Huang, *Statistical Mechanics* (Wiley, New York, 1987).

[6] M. Di Ventra, in *Electrical Transport in Nanoscale Systems* (Cambridge University Press, Cambridge, 2008), Chap. 8, pp. 376–414.

[7] H. Guo, E. Ilseven, G. Falkovich, and L. S. Levitov, Proc. Natl. Acad. Sci. USA **114**, 3068 (2017).

[8] J. Y. Khoo, P.-Y. Chang, F. Pientka, and I. Sodemann, Phys. Rev. B **102**, 085437 (2020).

[9] P. R. Roach and J. B. Ketterson, Phys. Rev. Lett. **36**, 736 (1976).

[10] M. J. M. de Jong and L. W. Molenkamp, Phys. Rev. B **51**, 13389 (1995).

[11] R. N. Gurzhi, Sov. Phys. Usp. **11**, 255 (1968).

[12] R. N. Gurzhi, A. N. Kalinenko, and A. I. Kopeliovich, Phys. Rev. Lett. **74**, 3872 (1995).

[13] D. T. Son, Phys. Rev. Lett. **98**, 020604 (2007).

[14] F. D. M. Haldane, arXiv:0906.1854.

[15] A. V. Andreev, S. A. Kivelson, and B. Spivak, Phys. Rev. Lett. **106**, 256804 (2011).

[16] C. Hoyos and D. T. Son, Phys. Rev. Lett. **108**, 066805 (2012).

[17] J. E. Avron, R. Seiler, and P. G. Zograf, Phys. Rev. Lett. **75**, 697 (1995).

[18] L. Levitov and G. Falkovich, Nat. Phys. **12**, 672 (2016).

[19] P. S. Alekseev, Phys. Rev. Lett. **117**, 166601 (2016).

[20] A. Principi, G. Vignale, M. Carrega, and M. Polini, Phys. Rev. B **93**, 125410 (2016).

[21] T. Scaffidi, N. Nandi, B. Schmidt, A. P. Mackenzie, and J. E. Moore, Phys. Rev. Lett. **118**, 226601 (2017).

[22] P. S. Alekseev and A. P. Alekseeva, Phys. Rev. Lett. **123**, 236801 (2019).

[23] D. A. Bandurin, I. Torre, R. Krishna Kumar, M. Ben Shalom, A. Tomadin, A. Principi, G. H. Auton, E. Khestanova, K. S. Novoselov, I. V. Grigorieva, L. A. Ponomarenko, A. K. Geim, and M. Polini, Science **351**, 1055 (2016).

[24] A. I. Berdyugin, S. G. Xu, F. M. D. Pellegrino, R. Krishna Kumar, A. Principi, I. Torre, M. Ben Shalom, T. Taniguchi, K. Watanabe, I. V. Grigorieva, M. Polini, A. K. Geim, and D. A. Bandurin, Science **364**, 162 (2019).

[25] G. Policastro, D. T. Son, and A. O. Starinets, Phys. Rev. Lett. **87**, 081601 (2001).

[26] T. Holder, R. Queiroz, and A. Stern, Phys. Rev. Lett. **123**, 106801 (2019).

[27] O. Golan, C. Hoyos, and S. Moroz, Phys. Rev. B **100**, 104512 (2019).

[28] F. Rose, O. Golan, and S. Moroz, SciPost Phys. **9**, 006 (2020).

[29] J. A. Sulpizio, L. Ella, A. Rozen, J. Birkbeck, D. J. Perello, D. Dutta, M. Ben-Shalom, T. Taniguchi, K. Watanabe, T. Holder, R. Queiroz, A. Principi, A. Stern, T. Scaffidi, A. K. Geim, and S. Ilani, Nature (London) **576**, 75 (2019).

[30] M. J. H. Ku, T. X. Zhou, Q. Li, Y. J. Shin, J. K. Shi, C. Burch, L. E. Anderson, A. T. Pierce, Y. Xie, A. Hamo, U. Vool, H. Zhang, F. Casola, T. Taniguchi, K. Watanabe, M. M. Fogler, P. Kim, A. Yacoby, and R. L. Walsworth, Nature (London) **583**, 537 (2020).

[31] J. Crossno *et al.*, Science **351**, 1058 (2016).

[32] G. M. Gusev, A. D. Levin, E. V. Levinson, and A. K. Bakarov, Phys. Rev. B **98**, 161303(R) (2018).

[33] A. D. Levin, G. M. Gusev, E. V. Levinson, Z. D. Kvon, and A. K. Bakarov, Phys. Rev. B **97**, 245308 (2018).

[34] P. J. W. Moll, P. Kushwaha, N. Nandi, B. Schmidt, and A. P. Mackenzie, Science **351**, 1061 (2016).

[35] I. Torre, A. Tomadin, A. K. Geim, and M. Polini, Phys. Rev. B **92**, 165433 (2015).

[36] L. Bockhorn, I. V. Gornyi, D. Schuh, C. Reichl, W. Wegscheider, and R. J. Haug, Phys. Rev. B **90**, 165434 (2014).

[37] R. Haug, Negative magnetoresistance in high-mobility heterostructures, Workshop: Quantum transport in 2D systems, Luchon, France, 2015, http://www.quantware.ups.tlse.fr/ecoledeluchon/sessionw2/program.html.

[38] Q. Shi, P. D. Martin, Q. A. Ebner, M. A. Zudov, L. N. Pfeiffer, and K. W. West, Phys. Rev. B **89**, 201301(R) (2014).

[39] F. M. D. Pellegrino, I. Torre, A. K. Geim, and M. Polini, Phys. Rev. B **94**, 155414 (2016).

[40] K. L. Shepard, M. L. Roukes, and B. P. Van der Gaag, Phys. Rev. Lett. **68**, 2660 (1992).

[41] D. Weiss, M. L. Roukes, A. Menschig, P. Grambow, K. von Klitzing, and G. Weimann, Phys. Rev. Lett. **66**, 2790 (1991).

[42] R. Kumar *et al.*, Nat. Phys. **13**, 1182 (2017).

[43] Z. Qian and G. Vignale, Phys. Rev. B **71**, 075112 (2005).

[44] G. M. Gusev, A. D. Levin, E. V. Levinson, and A. K. Bakarov, AIP Adv. **8**, 025318 (2018).

[45] In the large sized sample with $L = 5\,\mu$m and $d = 1\,\mu$m, a large peak of R_{xx} occurs near the zero B-field, which is consistent with the results with large L, i.e., in Ref. [10].